Study of process parameters on optical qualities for injection-molded plastic lenses

Huai En Lai and Pei Jen Wang*

Department of Power Mechanical Engineering, National Tsing Hua University, 101, Sec. 2, Kuangfu Road, Hsinchu 30013, Taiwan, Republic of China

*Corresponding author: pjwang@pme.nthu.edu.tw

Received 3 January 2008; revised 4 March 2008; accepted 7 March 2008; posted 10 March 2008 (Doc. ID 91177); published 11 April 2008

Numerical simulations for mold-flow analysis and experimental measurements of injection-molded plastic lenses have been conducted for investigation of optical qualities, residual birefringence, and form accuracy resulting from various pertinent process conditions. First, residual birefringence distributions on the lens have been predicted and verified experimentally. Furthermore, full-scale factorial design of experiments was conducted to comprehend the influences of qualities, such as shear stresses, form accuracy, and volumetric deviation, on the measured primary or Seidel aberrations. In conclusion, residual birefringence induced by stresses represented by photoelasticity measurements agrees well with the numerical predictions and the experimental results indicate that the residual birefringence is mainly generated during the mold-filling stage. In addition, spherical aberration of the injection-molded plastic lenses is more sensitive to the pertinent qualities as compared to coma and astigmatism.

OCIS codes: 260.1440, 080.1010, 220.3630, 080.2205.

1. Introduction

In this paper, comprehensive study of injection-molded plastic lenses is presented through both numerical simulations and experimental verifications for illustrating the pertinent optical characteristics of the plastic lenses. First, results from three-dimensional mold-flow analysis are employed to simulate the thermomechanical history of molten plastics inside the mold cavity in terms of stresses and shrinkage. Then, individual effects from the flow-induced and thermal-induced birefringence are investigated by photoelasticity measurements on thermally annealed lenses. Furthermore, with the help of Taguchi methods as design of experiment (DOE) steps for comprehending the processing influences of processing conditions on qualities including residual birefringence, form accuracy, and volumetric deviations. For further study of the effects of processing conditions and interactions among the qualities [1–5], a systematic method based upon factorial design of experiments is adopted for investigating the effects of residual birefringence, form accuracy, and volumetric deviations on the Seidel aberrations. The conclusions show prominent results and observations in the injection molding of plastic lenses.

Since Sir Isaac Newton published basic theories for light and optics in the 18th century, optical instruments have been invented and manufactured for exploring minute bioorganisms, distant planets, and even mysterious galaxies. As progress in optical engineering technology was made in the past few decades, optical lenses are commonly adopted by various consumer products for either capture or display of images. For examples, 3G mobile phones, digital still cameras, and digital video projectors all are equipped with modern optical lenses. Since consumer products are mass produced in thousands or millions of units monthly, cost reduction has become the major research objective in industries recently. In modern manufacture processes, the injection-molding process has been widely accepted because

0003-6935/08/122017-11$15.00/0

of its ability to meet stringent production requirements. However, compared to the glass lenses made by the grinding and polishing process, injection-molded plastic lenses have been known for poor production yields because the lenses are made by complex manufacture procedures which require thermal annealing for enhancing dimensional stability afterward. It has been noted that the quality of optical images in plastic lenses is influenced by two groups of crucial factors, namely, the one contributing to residual birefringence and the other to changing the mechanical dimensions. In general, the residual birefringence defocuses and blurs the optical image of objects designated by the modulation transfer function (MTF) requirements. Based upon the literature [6], the residual birefringence evidently has become a major design and production problem in high-density information storage medias and high resolution optical systems.

In photoelasticity theory for materials with isotropic optical properties, residual birefringence is described as linear characteristics between residual stresses and refractive indices of materials defined as follows [7]:

$$n_2 - n_1 = c(\sigma_1 - \sigma_2),$$
$$n_3 - n_2 = c(\sigma_2 - \sigma_3), \quad n_1 - n_3 = c(\sigma_3 - \sigma_1). \qquad (1)$$

In Eq. (1), σ_1, σ_2, and σ_3 are the principal residual stresses at the point of interest; n_1, n_2, and n_3 are the refractive indices of materials associated with the principal stress directions; and c is the stress optic coefficient. According to the literature [8–10], two mechanisms dominate the residual birefringence phenomena in injection-molded lenses; they are commonly known as the flow-induced and thermal-induced residual birefringence, respectively. The former is credited to frozen molecule orientations because of mechanical shear stresses occurring at the filling and holding stage; whereas the latter is attributed to shrinking stresses due to nonuniform cooling before part removal. It should be further clarified that the residual birefringence phenomena are dependent of time and temperature history because of the viscoelastic properties in polymeric materials.

In the past decades, many papers on analyzing the residual birefringence in complex injection-molding processes have been published for injection-molded disks approximated with the Hele–Shaw model [8–11]. However, the Hele–Shaw model is insufficient for representing the flow characteristics of lenses and moldings with microstructures because it is a two-dimensional model. As a result, dimensional errors of injection-molded lenses are still unpredictable through numerical simulations, and they contribute to the primary or Seidel aberrations in object image; namely, spherical aberration, coma, astigmatism, field curvature, and distortion.

In the progress of development in optical materials, a well-known polymeric material developed for optics applications, technically known as cycloolefin polymer (COP), has recently merged into mass production of plastic lenses in consumer products. Among the commercialized COP polymers, ZEONEX, produced by Zeon Chemicals, Japan, is specially tailored for optical lenses because of very low water absorption, low density, low impurity, high deflection temperature, and high transmittance. From the literature, most published works in the manufacture of plastic lenses have been conducted for polymethyl-methacrylate (PMMA) and polycarbonate (PC), but not for COP polymers. It is the goal of this paper to study the optical qualities in injection-molded ZEONEX plastic lenses with comprehensive experimental verification.

2. Manufacture Process Analysis

In this study, a commercial mold-flow analysis program MOLDEX3D, copyrighted by CoreTech System at Chupei, Taiwan, has been chosen for simulating the thermomechanical history of polymeric materials inside the mold cavity throughout the complete process. The main features of the program are iterative calculations of flow, pressure, and temperature values of molded lenses at various stages, such as filling, packing, cooling, and postcooling, with details described elsewhere [12–16]. More importantly, all the calculated results are displayed with the help of graphical postprocessors for thermal-mechanical history and distributions in various locations.

A. Mold-Flow Analysis

In the numerical simulations of the process, polymeric melt is assumed to be incompressible during the filling stage but compressible at the postfilling stage. And, the polymeric melt is characterized by the generalized Newtonian fluid model and described by governing equations for nonisothermal three-dimensional flow inside the mold cavity formulated as follows [14,15]:

$$\frac{\partial \rho}{\partial t} + \nabla.\rho\,\mathbf{u} = 0, \qquad \frac{\partial}{\partial t}(\rho\,\mathbf{u}) + \nabla.(\rho\,\mathbf{uu} - \sigma) = \rho g,$$
$$\boldsymbol{\sigma} = -pI + \eta(\nabla\mathbf{u} + \nabla\mathbf{u}^T),$$
$$\rho C_p\left(\frac{\partial T}{\partial t} + \mathbf{u}.\nabla T\right) = \nabla(k\nabla T) + \eta\dot{\gamma}^2, \qquad (2)$$

where $\mathbf{u}$ is the velocity vector; T is the temperature; t is the time; p is the pressure, σ the total stress tensor, ρ the density, η the viscosity, k the thermal conductivity, C_p the specific heat, and $\dot{\gamma}$ the shear rate. Based upon the physical phenomena of fluid mechanics, the polymeric melt driven by pressure-head would flow along the path with minimal flow resistance; that is, the longer the flow distance per unit time, the smaller the flow resistance along the flow path.

Since injection-molded parts would deform after the process, the MOLDEX3D/SOLID-WARP module has been adopted for warpage analysis of the three-dimensional injection-molded lenses. Based upon the thermal-elasticity theory of solid structures, the module treats three-dimensional stress–strain deformation problems as simple solid structures. In the analysis, pertinent assumptions are made for linear and elastic materials properties (1), small strains (2), and the static equilibrium structure (3). Hence, the equilibrium equation with σ representing the stress and F representing body forces plus thermal loads is written as

$$\nabla\sigma + F = 0. \tag{3}$$

The stress–strain relationship can be defined as

$$\sigma_{ij} = C_{ijkl}(\varepsilon_{kl} - \varepsilon_{kl}^{0} - \alpha_{kl}\Delta T) + \sigma_{ij}^{F} \quad \text{and}$$
$$\varepsilon_{\mathrm{ij}} = \frac{1}{2}(u_{i,j} + u_{j,i}), \tag{4}$$

where σ_{ij} is the stress component, σ_{ij}^{F} is the stress induced by flow, ε_{ij} is the infinitesimal elastic strain component, ε_{ij}^{0} is the initial strain from pressure-volume-temperature effects, C_{ijkl} is the elastic material stiffness, α_{kl} is the coefficient of linear thermal expansion, and ΔT is the temperature difference.

Before the flow analysis, geometric models first have to be established by the use of the RHINO CAD program, copyrighted by Robert McNeel & Associates, USA. The geometric data of an aspheric lens and the relevant mesh model are shown in Figs. 1 and 2. Then, mesh information was exported to MOLDEX3D for flow analysis. In the flow analysis, the material properties, pertinent processing conditions, and simulation control parameters are properly selected as reported elsewhere [17,18]. As for calculations of volumetric shrinkage, the thermodynamic properties of the materials are employed for selected locations of the molded lenses, defined as

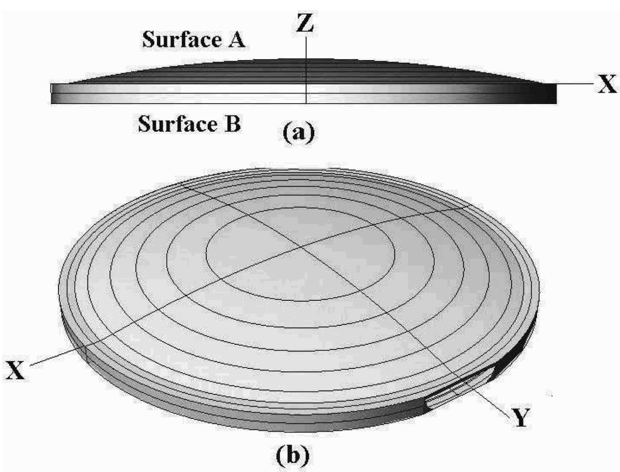

Fig. 1. Schematic drawings of sample aspheric lens: (a) surface A is spherical in 70.35 mm with surface B being aspheric, (b) perspective view of the lens with 30 mm in diameter and 2 mm in thickness.

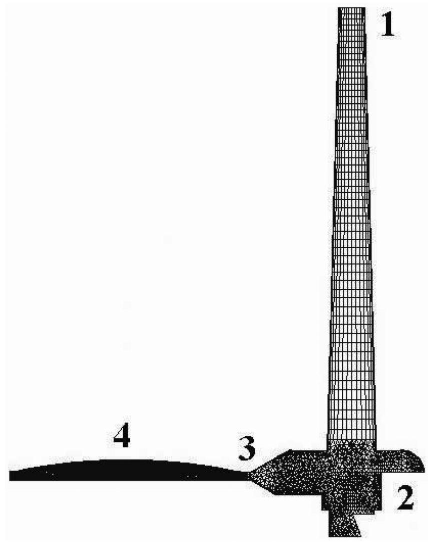

Fig. 2. Geometric drawing of the (1) sprue, (2) runner, (3) gate, and (4) lens cavity modeled with tetrahedral and prism mesh employed for the simulations.

$$Sv = \frac{Vc - V}{Vc} = 1 - \frac{V}{Vc}, \tag{5}$$

where Vc is the specific volume at room temperature and V is the specific volume after ejection. Figure 3(a) shows that the largest volumetric shrinkage happens at the center of the molded lenses because a higher melt temperature resides at the center. Moreover, part warpage is the result of nonuni-

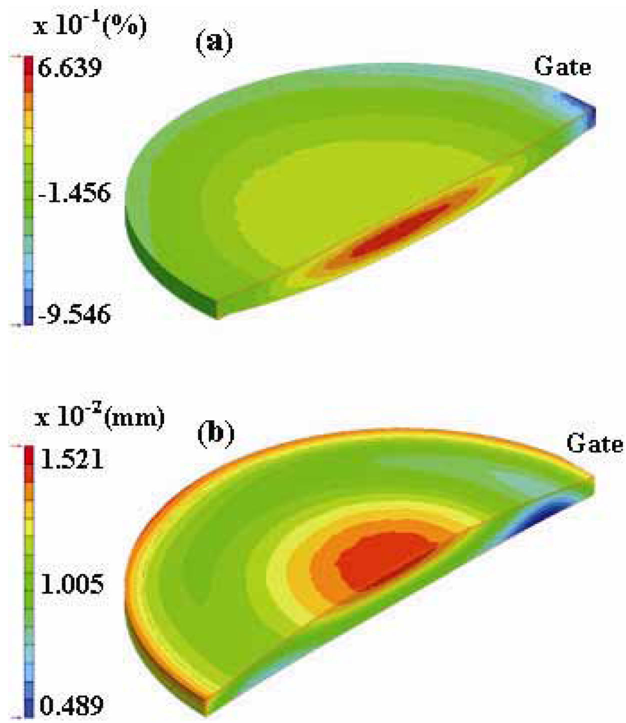

Fig. 3. (Color online) Three-dimensional shaded plots in cut-view of simulation results: (a) volumetric shrinkage and (b) warpage after ejection.

form volumetric shrinkage in molded lenses at the cooling stage. That is, variations of temperature and pressure induce corresponding changes in specific volume of molded lenses. Therefore, a lot of factors, such as materials properties, part design, mold design, and processing conditions, would have significant influences on the waprage of parts. Figure 3(b) illustrates that the periphery portions of molded lenses deform upward significantly while the center portions deform downward.

B. Experimental Verifications

To validate the accuracy of simulation results, experimental verifications were conducted on photoelasticity measurements. In the measurements, residual birefringence within the lenses was measured by making use of a circular polariscope [7]. To illustrate the principle of photoelasticity measurement, Fig. 4 shows the arrangement of various optical components in the apparatus. In the figure, the mathematical expression for the light rays emerging out from the analyzer can be written as

$$E_{ax} = k \times \sin\frac{\Delta}{2}\sin\left(\omega t + 2\alpha - \frac{\Delta}{2}\right). \tag{6}$$

Since the intensity of light is proportional to the square of the amplitude of the light rays, the light intensity emerging from the analyzer is given by

$$I = K \times \sin^2\frac{\Delta}{2}. \tag{7}$$

From Eq. (7), the intensity of the light rays is a function of the principal stress difference Δ. The $\sin^2(\Delta/2)$ term shows that intensity extinction would occur when $\Delta/2 = n\pi$, where $n = 0, 1, 2, 3, \ldots$ [7].

From the experimental results, Fig. 5(a) shows the residual birefringence and shear stress levels near the gate in molded lenses are much higher. The fringe patterns of the molded lenses are in good agreement with shear stress distributions at the end of filling stage. For further investigation of the results, simulated sensor nodes placed along the filling path at equal distance are selected in the lens to record the history of the filling and packing stage, as shown in Fig. 5(b). Then it is noted that shear stresses decrease along the path away from the gate at path 3; similar trends at other paths are also observed as shown in Fig. 5(c). Again, the simulation results for shear stress distributions during the filling stage agree well to the photoelasticity measurements. The rationale for the above conclusion can be explained in the followings.

At first, total stress tensor in molded lenses at the end of filling stage can be expressed as

$$\sigma = \begin{bmatrix} -P + \sigma_{11} & \sigma_{12} & \sigma_{13} \\ \sigma_{21} & -P + \sigma_{22} & \sigma_{23} \\ \sigma_{31} & \sigma_{32} & -P + \sigma_{33} \end{bmatrix}, \tag{8}$$

where $\sigma_{12}, \sigma_{13}, \sigma_{21}, \sigma_{23}, \sigma_{31}$, and σ_{32} are shear stresses; σ_{11}, σ_{22}, and σ_{33} are normal stresses; and P is the pressure. Because the lens profile can be treated as a circular plate, stresses in the z direction compared with the stresses in the x and y directions are smaller and assumed to be negligible. Equation (8) reduces to a two-dimensional matrix as

$$\sigma = \begin{bmatrix} -P + \sigma_{11} & \sigma_{12} \\ \sigma_{21} & -P + \sigma_{22} \end{bmatrix}. \tag{9}$$

The residual birefringence in the xy plane can be calculated based upon the stress optic law, defined as [19]

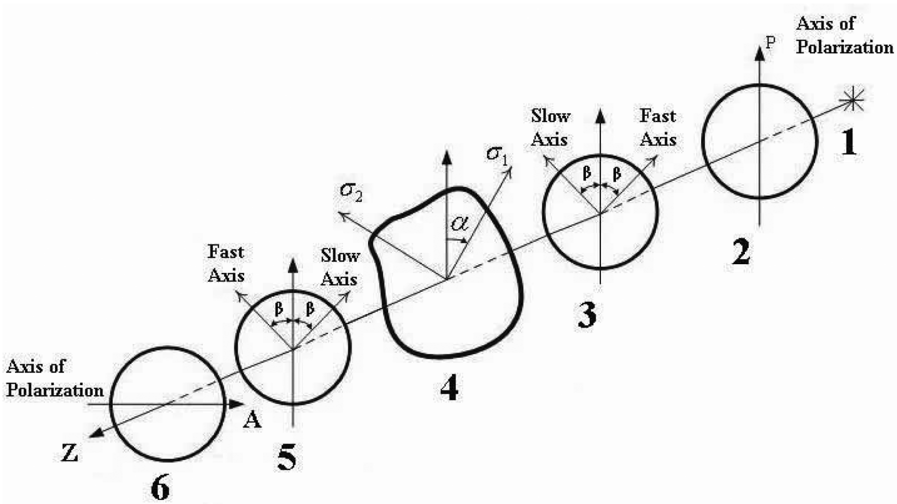

Fig. 4. Schematic illustration of photoelasticity measurements: 1 is the light source; 2 is the polarizer; 3 is the first quarter-wave plate, where β is $\pi/4$; 4 is the sample lens, where α is the principal-stress direction making an angle with the axis of polarization of the polarizer; 5 is the second quarter-wave plate; and 6 is the analyzer [7].

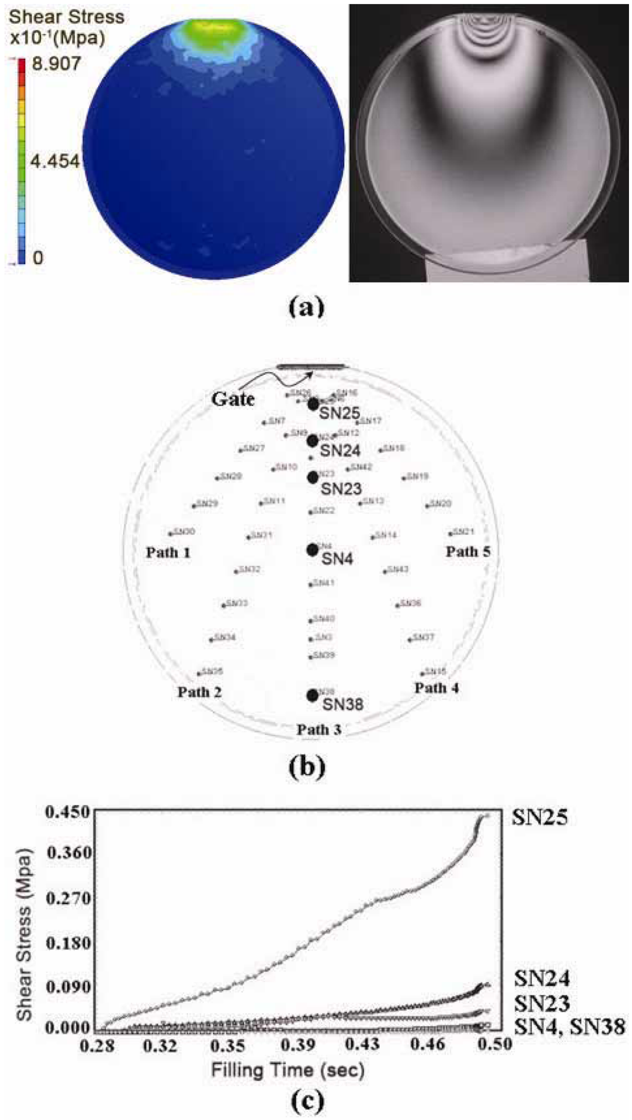

Fig. 5. (Color online) Comparisons between predicted shear stresses and fringe patterns: (a) shear stresses distribution versus fringe patterns, (b) locations of sensor nodes in the lens cavity, and (c) plots of shear stresses for sensor nodes at path 3 versus time during filling stage.

$$\Delta n = c(\sigma_1 - \sigma_2) = c\sqrt{(\sigma_{11} - \sigma_{22})^2 + 4\sigma_{12}^2}, \qquad (10)$$

where σ_1 and σ_2 are principal stresses and c is the stress optic coefficient. In Eq. (10), the term $(\sigma_{11} - \sigma_{22})$ is zero because of isobaric pressure conditions for generalized Newtonian fluid (GNF) model flow [20]. That is,

$$\Delta n = c(\sigma_1 - \sigma_2) = 2c\sigma_{12}. \qquad (11)$$

In other words, residual birefringence is linearly dependent of shear stresses in the xy plane characterized by the stress optic coefficient. Hence, shear stresses during the filling stage should be effectively reduced by optimization of process parameters for lower residual birefringence.

3. Experimental Investigation of Birefringence

In the injection-molding process, two types of residual birefringence are observed in the moldings; namely, the flow-induced and the thermal-induced birefringence. In the following sections, the combined effects from both the flow-induced and thermal-induced birefringence are compared by the results from thermal annealing experiments together with photoelasticity measurements. In addition, birefringence distributions in the gapwise direction near gate area are verified by a layer-removal technique to further support the flow-induced effects.

A. Relaxation of Birefringence

For relaxation of thermal-induced effects, molded lenses were placed into a temperature-controlled oven for annealing the thermal-induced residual birefringence. According to the ASTM standards, heat deflection temperature (HDT) of ZEONEX 480R is 123 °C, according to the manufacture's datasheet. Hence, the oven temperature was set at 125 °C for 12 h at atmospheric pressure. After the samples were cooled, they were observed under a circular polariscope for measuring the differences [7]. From the fringes counted on the annealed lenses, it is difficult to notice the differences, as shown in Fig. 6. In conclusion, residual birefringence in the molded lenses was mainly attributed to the flow-induced effects during the process. Based upon measured data from photoelasticity measurements, the flow-induced effects account for 92.3 % of the total residual birefringence. As a further step for experimental verification, a birefringence analyzer, model Kobra 21ADH made by OSI Co., Japan, was employed for measuring the residual birefringence before and after the thermal annealing process. The results indicated a 4.17 % decrease in residual birefringence and confirmed the conclusion that thermal-induced effects in the cooling stage are negligible in the final birefringence results.

Since the residual birefringence has been proved to be dominated by the flow-induced effects, it is

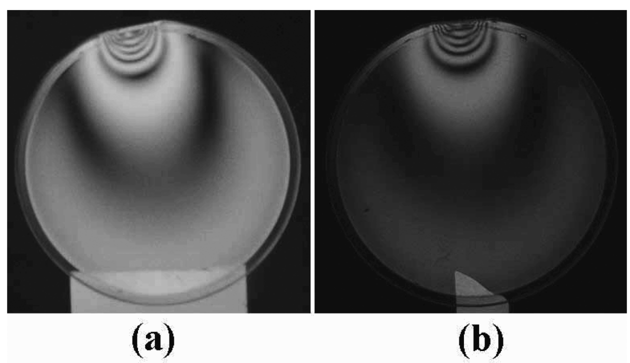

Fig. 6. Comparisons of annealing effects, where annealing temperature was set at 125 °C with annealing time being 12 h, on fringe orders before annealing and after annealing: (a) before annealing processes, fringe order is 6.5; and (b) after annealing processes, fringe order is 6.5.

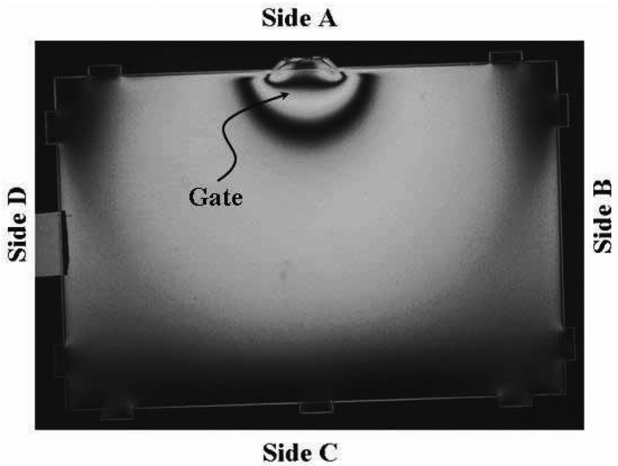

Fig. 7. Experimental results of linear shrinkage for sample plate at 125 °C for 12 h: after annealing processes, linear shrinkage at side A, side B, side C, and side D are $8.34 \times 10^{-2}\%$, $5.00 \times 10^{-2}\%$, $1.67 \times 10^{-2}\%$, and $7.50 \times 10^{-2}\%$, respectively.

necessary to study the effects of residual stresses on dimensional variations by experiments on sample plates via the thermal annealing process. The experimental results show that the shrinkage in percentile of the samples decreases with the distance from the gate, as shown in Fig. 7. Furthermore, more annealing experiments were conducted for molded lenses under various time periods and with the oven temperature set at 15 °C higher than the glass transition point (Tg), as shown in Fig. 8. In the figure, the photographs show that the gate area deforms significantly because of high residual stresses or birefringence. Hence, stress relaxation, as well as dimensional shrinkage, is severe for the annealed lenses at the gate area [21].

B. Birefringence Distributions

Based upon the conclusions from the previous section, residual birefringence distributions resulting from residual stresses must be carefully studied. Spherical lenses in planoconvex geometry with curvature of 70 mm, diameter of 32 mm, thickness of 2 mm, and gate thickness of 0.80 mm were molded for further experimentation, as shown in Fig. 9, with the corresponding process conditions being

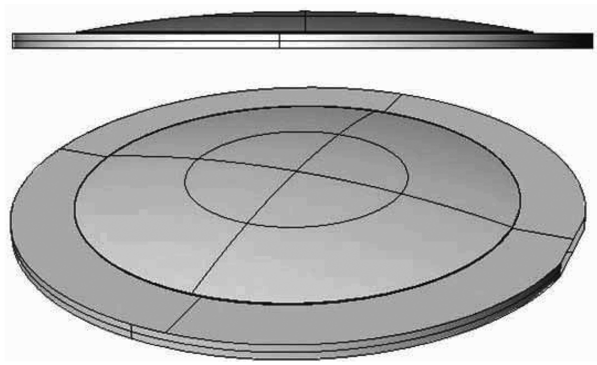

Fig. 9. Schematic drawings of the planoconvex spherical lens. The surface curvature is 70 mm with the diameter of 32 mm at thickness of 2 mm, while the gate is 0.80 mm in thickness.

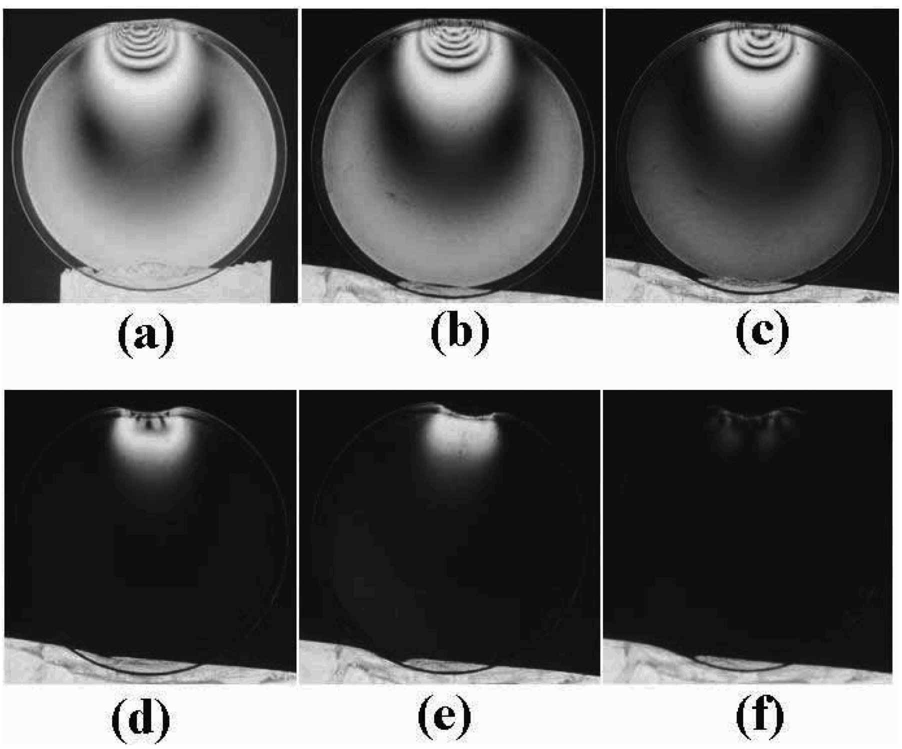

Fig. 8. Experimental results of lenses being annealed at 153 °C: (a) no annealing, (b) after 30 min annealing, (c) after 1 h annealing, (d) after 2 h annealing, (e) after 4 h annealing, and (f) after 8 h annealing.

Table 1. Pertinent Process Conditions for Computer-Aided Engineering Simulations and Experimental Verifications for Planoconvex Spherical Lenses

Process Conditions			
Machine Conditions	Clamping force	550	kN
	Injection weight	27	Gm
	Maximum pressure	259	Mpa
	Maximum flow	190	cc/sec
	Screw diameter	22	mm
	Stroke	70	mm
	Injection speed	22	mm/sec
	Holding pressure	98.10	Mpa
Mold Conditions	Cooling time	60	sec
	Open time	8.76	sec
	Coolant	Silicone oil	
	Room temperature	25	°C
Melt Conditions	Materials	Zeonex 480R	
	Melt temperature	275	°C
	Mold temperature	124	°C
	Ejecting temperature	127	°C

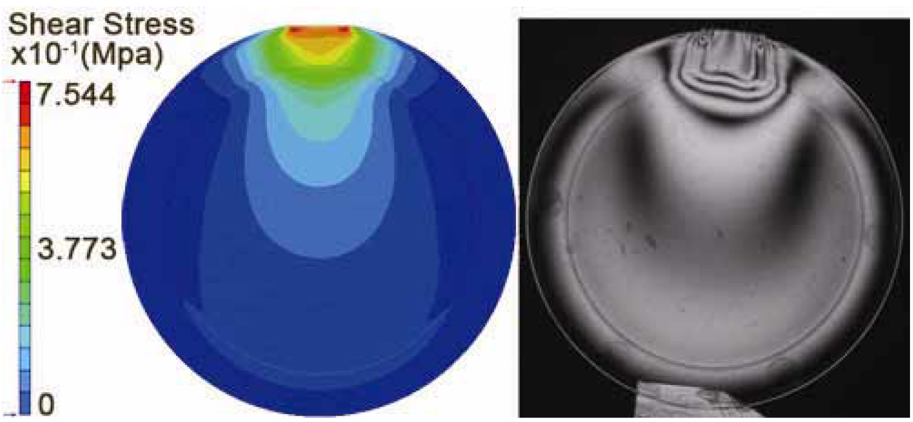

Fig. 10. (Color online) Comparisons between shear stresses distributions and residual birefringence distributions on the plano-convex spherical lenses.

illustrated in Table 1. In Fig. 10, the simulated distributions are in good agreement with the measured residual birefringence showing the trend of a decrease in residual stresses along the filling path.

As in the gapwise direction, it is noted that high residual stresses would occur near the lens surfaces, especially at the gate area, as shown in shaded plots of Fig. 11, and as predicted by the numerical simulations. As for experimental verification, a conventional layer-removal technique was used for removing layers of materials with residual stresses, as illustrated in Fig. 12. In the experiments, four

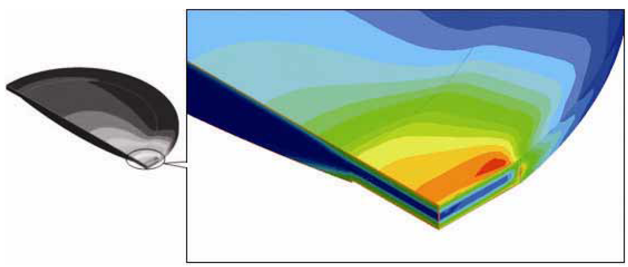

Fig. 11. (Color online) Shaded plots of predicted residual stresses in cut-view with enlarged insert in gapwise direction showing the high stresses near lens surfaces.

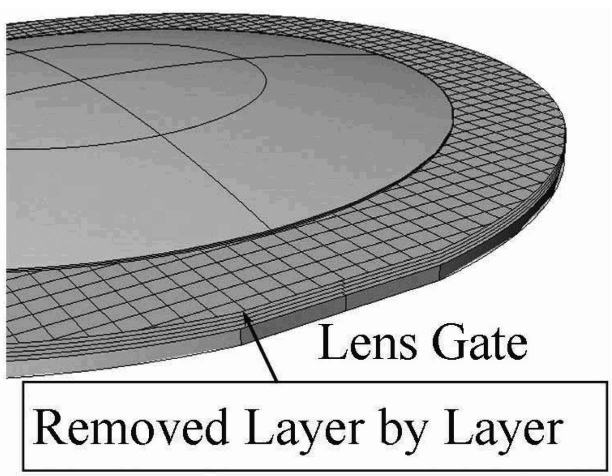

Fig. 12. Schematic drawing for illustrating the layer-removal technique applied to molded lenses.

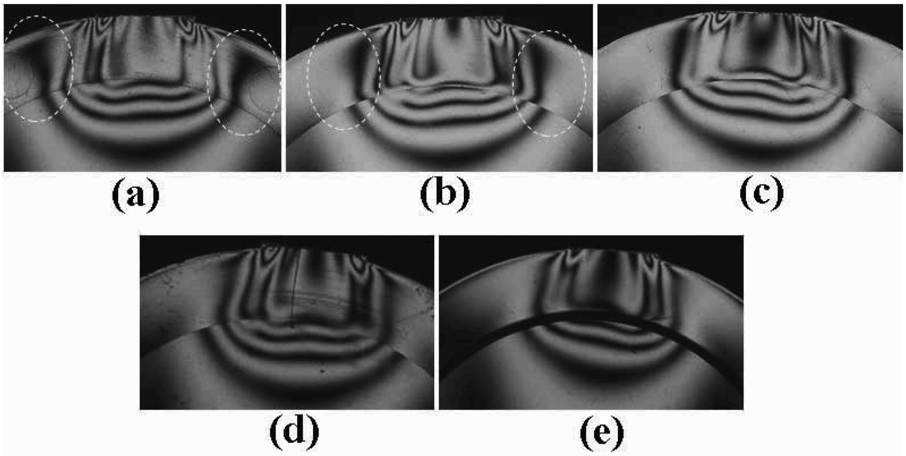

Fig. 13. Photographs of residual birefringence on samples prepared by layer-removal technique: (a) lens without machining, (b) lens with 0.1 mm removed, (c) lens with 0.2 mm removed, (d) lens with 0.3 mm removed, and (e) lens with 0.4 mm removed.

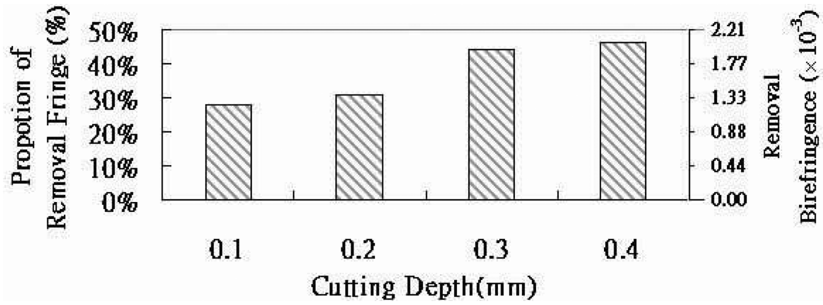

Fig. 14. Chart for percentile in removed birefringence versus thickness removed from the surface near the gate area.

samples of molded lenses with the same process conditions were carefully machined by diamond turning in layer thickness of 0.1 mm, 0.2 mm, 0.3 mm, and 0.4 mm, respectively. Figure 13 compares the photographs of residual birefringence under various removed layers. In Fig. 13(a), level of residual birefringence changes significantly after the 0.1 mm layer is removed. For further illustration on the change of residual birefringence in gapwise direction, the average fringe order of the sample lenses was measured and plotted in percentile of removal, as shown in Fig. 14. It should be noted that nearly 30% of birefringence was removed on the first 0.1 mm of materials. Fifty percent of the birefringence was removed for the case of 0.4 mm, which is half of total thickness at the gate area. Hence, from both the simulated and experimental results, most residual birefringence that would occur near the lens surfaces is confirmed. The rationale for this result is that polymer molecules are frozen in instantly in the surface layer when the hot melt contacts the cold mold wall during the filling stage, and that higher shear stresses would be needed to drive the melt forward hereafter.

4. Analysis of Qualities and Molding Conditions

Wang and Lai [17,18] reported results showing that four interactions on holding pressure with injection speed, mold temperature, melt temperature, and cooling time have little influence on shear stresses, which are mainly contributed by melt temperature and injection speed. Average volumetric deviations are mainly dependent of holding pressure and melt temperature. As for form accuracy, five main factors, including melt temperature, mold temperature, injection speed, holding pressure, and cooling time, are chosen for DOE factors with three-level settings, as shown in Table 2. Consequently, four interaction effects from melt temperature with mold temperature, injection speed, holding pressure, and cooling time, respectively, also were accounted for. Then, form accuracy of the molded lenses was measured by the Form Talysurf profiler, made by Taylor Hobson Ltd., U. K. The measured data were analyzed on the causal effects between the form accuracy and processing parameters. Because the form accuracy is interpreted in peak-to-valley (P-V) values, it should be minimized with an index with smaller-the-better (STB) characteristics as

$$\mathrm{SNR_{STB}} = -10\log\left(\frac{1}{n}\sum_{i=1}^{n} y_i^2\right), \qquad (12)$$

where n is the total number of measured values at each run process and y_i is the P-V value for each run process.

Table 2. Control Factors and Settings for DOE Analysis on Form Accuracy

Control Factors and Settings			
A	Melt Temperature (°C)	Level 1	247.5
		Level 2	275.0
		Level 3	280.0
B	Mold Temperature (°C)	Level 1	111.6
		Level 2	124.0
		Level 3	136.4
C	Injection Speed (mm/ sec)	Level 1	19.8
		Level 2	22.0
		Level 3	24.2
D	Holding Pressure (Mpa)	Level 1	88.29
		Level 2	98.10
		Level 3	107.91
E	Cooling Time (sec)	Level 1	54
		Level 2	60
		Level 3	66

The results of data analysis show that form accuracy is mainly affected by mold temperature and melt temperature plus holding pressure interaction. Form accuracy can be improved by increase in the melt temperature. This is because higher mold temperature would lessen the rapid cooling effects of polymer melt inside the mold cavity. Hence, the molded lenses can be better packed into higher form accuracy. Since the interaction of melt temperature and holding pressure is also important, the settings of melt temperature and holding pressure should be properly matched for high form accuracy, too.

5. Seidel Aberrations Measurements

Since it is already concluded that residual birefringence is mainly dependent of melt temperature and injection speed, form accuracy is primarily affected by mold temperature, and volumetric deviations are mostly caused by holding pressure as illustrated in Table 3. Based upon the conclusions, a full-scale factorial design of experiments can be scheduled for studying the effects of birefringence, form accuracy, and volumetric deviations on the Seidel aberrations; namely, astigmatism, coma, and spherical aberration. Table 4 shows all main factors and interactions with corresponding settings employed for the DOEs. In measuring the aberrations, a ZYGO GPI XP interferometer system is adopted for calculation of Zernike coefficients and the corresponding values for astigmatism, coma, and spherical aberration [22]. After five sample lenses are measured for average aberrations on each run, the data are plotted in Fig. 15, in which all aberrations are less than two wavelengths with spherical aberration being the most scattered data.

After data analysis with ANOVA (analysis of variance) processes are done, the contributions of the

Table 3. Relationships between Qualities and Process Conditions

Qualities	High Birefringence	High Form Accuracy	High Volumetric Deviations
Process Conditions	Low melt temperature High injection speed	High mold temperature	High holding pressure

Table 4. Full-scale Factorial Design of Experiments for Studying Effects of Qualities on Seidel Aberrations

	A. Birefringence		B. Form Accuracy	C. Volumetric Deviations
	Melt temperature	Injection speed	Mold temperature	Holding Pressure
Run	(°C) −(247.5) +(280.0)	(mm/ sec) −(19.8) +(22.4)	(°C) −(111.6) +(136.4))	(Mpa −(88.29) +(107.91)
1	−	+	−	−
2	−	+	−	+
3	+	−	+	−
4	+	−	+	+
5	−	+	+	−
6	−	+	+	+
7	+	−	−	−
8	+	−	−	++

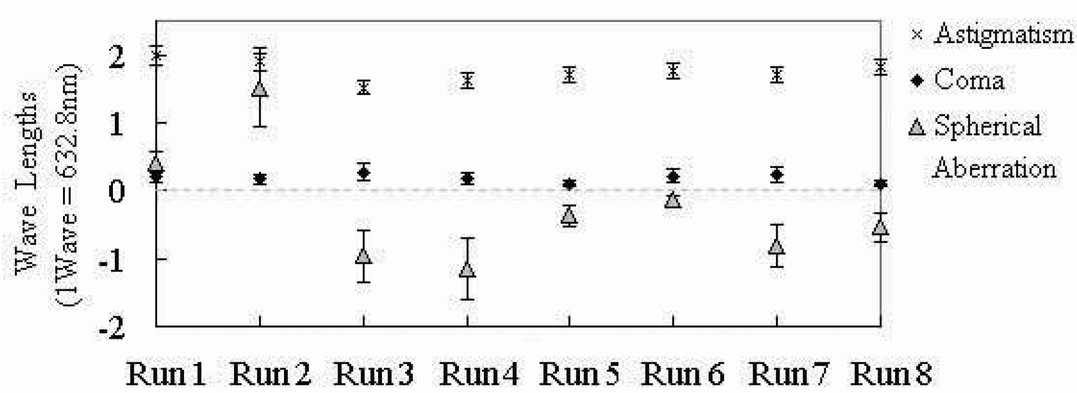

Fig. 15. Plots of average primary aberrations versus various process runs from the results of design of experiments.

Table 5. Contributions of Main Factors as Qualities on Seidel Aberrations

Astigmatism		Coma		Spherical Aberration	
Main factors	Contribution	Vital factors	Contribution	Vital factors	Contribution
A	41%	AB	24%	A	56%
B	40%	BC	22%	B	24%
others	19%	AC	14%	others	20%
		others	40%		

main factors and interactions can be tabulated in Table 5. It is noted that both form accuracy and birefringence are important in measured aberrations, especially in spherical aberration and astigmatism. On the contrary, volumetric deviations show less influence on aberrations. Therefore, effects from birefringence and form accuracy on primary aberrations cannot be eliminated after all. As for astigmatism, low birefringence and high form accuracy would directly reduce astigmatism. The rationale for the results will be discussed in Section 6. Based upon the results from aberration measurements, for molded lenses with birefringence with high form accuracy, it is still impossible to optimize aberrations by simply adjusting process conditions. However, for lenses with good optical design, small residual birefringence and high form accuracy could reduce primary aberrations more effectively.

6. Summary

The effects of process parameters on optical qualities for injection-molded lenses have been comprehensively studied by numerical simulations for mold-flow analysis and experimental verification conducted via the Taguchi methods with emphasis on residual birefringence, form accuracy, and volumetric deviations of the lenses. From the application of photoelasticity theory, residual birefringence in terms of residual stresses in plastic lenses made of COP polymers is carefully characterized. For residual birefringence, the measured data agree well with the simulation results and the data clearly indicate that residual birefringence is mainly attributed to flow-induced effects during the filling and packing stage. Moreover, residual birefringence distributions in gapwise direction have been predicted by simulations and verified by layer-removal experimental technique. It is concluded that major residual stresses or birefringence would occur near the lens surfaces, especially at the gate area.

From the results of the DOE, birefringence because of residual stresses is found to be mostly affected by melt temperature and injection speed among the pertinent process parameters, and average volumetric deviations are found to be credited to the holding pressure and melt temperature. Moreover, lens form accuracy is mainly affected by mold temperature and melt temperature plus holding pressure interaction. Furthermore, full-scale factorial design of experiments on the Seidel aberrations has been conducted for investigating effects of lens qualities. In conclusions, both form accuracy and residual birefringence contributed by residual stresses would be dominant in the measured aberrations; namely, spherical aberration, coma, and astigmatism. Because coma and astigmatism are measured when a lens is either in nonrotational symmetry or in nonparaxial ray conditions, the current method of measurements cannot identify the causal effects from the process conditions for the molded lenses. However, two conjectures are made in conclusion to explain why spherical aberration is more sensitive to qualities than astigmatism and coma are. The first conjecture is that the effects of thickness and shape for the outer region of the molded lenses were not accounted for in the DOE. Therefore, the bending effects on lens shape could have prominent influences on spherical aberrations, but not on astigmatism and coma. The second conjecture is that residual stresses play an important role (nearly 56% in total) on spherical aberration alone; whereas, the residual stresses affected by melt temperature and injection speed are so significant on the bending of lens shape. These two conjectures help explain why spherical aberration is more sensitive to qualities than the other two aberrations do. Finally, this paper has illuminated some possible remedies for process improvements on the manufacture of plastic lenses in the future.

The authors thank colleague C. H. Chen for his valuable discussions during the research periods. This research is supported by the National Science Council in Taiwan, the Republic of China, under contract No. NSC95-2221-E007-079.

References

1. X. H. Lu and L. S. Khim, "A statistical experimental study of the injection molding of optical lenses," J. Mater. Process. Technol. **113**, 189–195 (2001).
2. D. C. Montgomery, *Design and Analysis of Experiments* (Wiley, 2001).
3. J. Antony and F. J. Antony, "Teaching the Taguchi method to industry engineers," Work Study Manag. Services **50**, 141–149 (2001).
4. A. W. McFarland and J. S. Colton, "Production and analysis of injection molded micro-optic components," Polym. Eng. Sci. **44**, 564–579 (2004).
5. A. Bendell, J. Disney, and W. A. Pridmore, *Taguchi Methods: Applications in World Industry* (IFS, 1989).
6. Y. Maekawa, M. Onishi, A. Ando, S. Matsushima, and F. Lai, "Prediction of birefringence in plastics optical elements using 3D CAE for injection molding," Proc. SPIE **3944**, 935–943 (2000).
7. J. W. Dally and W. F. Riley, *Experimental Stress Analysis* (McGraw-Hill, 1991).
8. K. Yoon, "An experimental study on precision injection molding of center-gated disks," Korean J. Rheol. **7**, 19–27 (1995).
9. G. D. Shyu, A. I. Isayev, and H. S. Lee, "Numerical simulation of flow-induced birefringence in injection molded disk," Korea-Australia Rheol. J. **15**, 159–166 (2003).
10. B. F. Fan, D. O. Kazmer, W. C. Bushko, R. P. Theriault, and A. J. Poslinski, "Birefringence prediction of optical media," Polym. Eng. Sci. **44**, 814–824 (2004).
11. C. A. Hieber and S. F. Shen, "Flow analysis of the non-isothermal two-dimensional filling process in injection molding," Isr. J. Technol. **16**, 248–254 (1978).
12. S. Y. Kim, M. H. Rim, W. S. Lim, and W. Y. Kim, "A numerical approach for optical characteristics of injection-molded lens," in *Proceedings of ANTEC 1999 Plastics: Bridging the Millennia*, (Society of Plastics Engineers, 1999), pp. 1491–1495.
13. C. H. Chien, Y. Maekawa, H. Kishikawa, M. Onishi, and F. S. Lai, "Influence of processing conditions on the formation of birefringence of optical plastics lens by using 3D CAE," in *Proceedings of ANTEC 2001 Plastics: The Lone Star* (Society of Plastics Engineers, 2001), pp. 1338 – 1342.
14. R. Y. Chang and W. H. Yang, "Numerical simulation of mold filling in injection molding using a three-dimensional finite volume approach," Int. J. Numer. Methods Fluids **37**, 125–148 (2001).
15. A. Y. Peng, W. H. Yang, and D. C. Hsu, "Enhanced structure CAE solution with molding effect for automotive parts," in *Proceedings of ANTEC 2005 Plastics* (Society of Plastics Engineers, 2005), pp. 2787 – 2791.
16. L. S. Turng, M. Peic, and D. K. Bradley, "Process simulation and optimization for injection molding-experimental verifications and field applications," J. Inj. Molding Technol. **6**, 143–155 (2002).
17. P. J. Wang and H. E. Lai, "Study of optical characteristics for injection molded aspheric lenses," in *Proceedings of Asia Pacific Conference on Optics Manufacture* (Asia Pacific Conference on Optics Manufacture, 2007).
18. P. J. Wang and H. E. Lai, "Study of residual birefringence in injection molded lenses," in *Proceedings of Plastics Encounter at ANTEC 2007* (Society of Plastics Engineers, 2007), pp. 2494 – 2498.
19. H. Janeschitz-Kriegl, *Polymer Melt Rheology and Flow Birefringence* (Spring-Verlag, 1983).
20. R. B. Bird, R. C. Armstrong, and O. Hassager, *Dynamics of Polymeric Liquids* (Wiley, 1987).
21. P. B. John, *Runner and Gating Design Handbook* (Hanser, 2004).
22. J. C. Wyant, *Applied Optics and Optical Engineering, Vol. XI* (Academic, 1992).